Extreme Mechanics Letters 41 (2020) 101031

Contents lists available at ScienceDirect

Extreme Mechanics Letters

journal homepage: www.elsevier.com/locate/eml

Elastic modulus mapping for bovine cortical bone from submillimeter- to submicron-scales using PeakForce Tapping atomic force microscopy

Yuxiao Zhou [a], Markus J. Kastner [b], Timothy B. Tighe [b], Jing Du [a,*]

[a] Department of Mechanical Engineering, Pennsylvania State University, University Park, PA, United States of America
[b] Materials Research Institute, Pennsylvania State University, University Park, PA, United States of America

ARTICLE INFO

Article history:
Received 14 July 2020
Received in revised form 6 September 2020
Accepted 11 October 2020
Available online 13 October 2020

Keywords:
Cortical bone
Atomic force microscopy
Elastic modulus
PeakForce Tapping

ABSTRACT

Bone is a composite material consisting of organic and inorganic components that are organized into hierarchical structures to provide load-bearing functions. This paper presents the results of PeakForce Tapping atomic force microscopy (AFM) scans on cut and polished bovine cortical bone specimens that were submerged in water. The elastic modulus map and surface morphology were obtained for various bone hierarchical structures from submillimeter- to submicron-scales. The elastic modulus of osteons (20.51 ± 6.85 GPa) was slightly lower than the interstitial bone (21.87 ± 5.48 GPa); they were both much greater than that of the cement lines (7.49 ± 4.23 GPa). The elastic modulus in the lamella structures varied periodically from higher values in thick sub-lamellae (21.49 ± 6.58 GPa) to the lower values in thin sub-lamellae (9.67 ± 2.69 GPa). The results also show relatively softer mineralized collagen fibril bundle arrays (12.94 ± 2.71 GPa) embedded in harder matrix materials (28.39 ± 5.75 GPa). The variations in the elastic modulus suggest different degrees of mineralization or different fibril orientations. The histograms of elastic modulus indicate the dominating compositions or dominating fibril orientations.

1. Introduction

Bone is a composite material consisting of organic and inorganic components. The organic component is mostly collagen; the inorganic component is mostly bioapatite minerals. These two components organized into hierarchical structures from nano- to macro-scales that provide load-bearing functions.

In prior works, several different techniques have been applied to measure the elastic properties of bone structures at various scales. These methods include tension test on millimeter-scale bone specimens [1], ultrasonic measurement on millimeter-scale bone specimens [2,3], 3-point bending of sub-millimeter bone specimens [4], push-out test of sub-millimeter single osteons [5–7], acoustic microscopy that have spatial resolution of several dozen microns [8,9], and nanoindentation techniques that measures the elastic modulus of sub-millimeter osteons and interstitial bone [10] and the micro-scale thick and thin sub-lamellae [11].

Atomic force microscopy (AFM) can be used to characterize surface morphology with nano-scale features. It has been used to measure the width of bone lamellae [12], the shape and size of isolated bone mineral particles [13–15], and the diameter of collagen fibrils [14–16]. AFM has also been used in the mechanical testing, including AFM-based tension test of single collagen fibrils [17,18] and AFM-based nanoindentation of bone and cartilage [19,20].

PeakForce Tapping AFM enables elastic modulus mapping with nano-scale spatial resolution. In this work, PeakForce Tapping AFM was used to scan the surface of cut and polished bovine cortical bone specimens that were submerged in water. AFM scans with several different sizes were obtained. The elastic modulus and surface morphology were obtained for bone hierarchical structures from sub-millimeter to sub-micron-scales. The structural and compositional variations that may underly the variations in the measure elastic moduli were discussed.

2. Material and method

2.1. Sample preparation

Fresh bovine long bones were obtained from Pennsylvania State University Meats Laboratory. The soft tissues, including bone marrow, were removed mechanically. They were first cut into several strips along the long axis of the bone by a cutting blade. The strips dominated by the haversian bone were used in the following experiments. They were sectioned into thin slices in the transverse plane perpendicular to the long axis of the bone

* Correspondence to: Penn State University, 316B Leonhard Building, University Park, PA 16802, United States of America.
E-mail addresses: yyz5239@psu.edu (Y. Zhou), muk303@psu.edu (M.J. Kastner), tbt1@psu.edu (T.B. Tighe), jingdu@psu.edu (J. Du).

https://doi.org/10.1016/j.eml.2020.101031
2352-4316/

by a precision saw with a diamond blade (Isomet 1000 Precision Cutter, Buehler, Lake Bluff, IL). Each bone specimen had an area of about 10 mm × 10 mm in the transverse plane and a thickness of about 1.5 mm in the longitudinal direction.

The bovine bone specimens were polished by a grinder polisher (EcoMet 30, Buehler, Lake Bluff, IL) first using silicon carbide grinding papers with progressively finer grit of 800 and 1200 and then using diamond suspension with grades of 6, 3, 1, 0.25 and 0.1 μm, respectively, on silk polishing cloths (South Bay Technologies, San Clemente, CA and SMS Labs, Sturbridge, MA). After each round of polishing, the bone specimens were cleaned by ultrasonic bath (Branson Ultrasonics, Danbury, CT) in deionized (DI) water for 2 min to remove the polishing residues. The polished and cleaned specimens were glued onto plastic petri dish using epoxy resin, and was kept moisturized in Kimwipes (Kimberly-Clark, Irving, TX) soaked with modified Hanks' Balanced Salt Solution (HBSS) (Sigma Aldrich, St. Louis, MO) until testing.

2.2. Peakforce tapping AFM

The surface profiles and the elastic modulus map of the polished surfaces on the bone specimens were measured using an AFM (BioScope Resolve, Bruker, Billerica, MA) under PeakForce Tapping mode. Etched silicon AFM probes (RTESPA-525, Bruker, Billerica, MA) with a nominal spring constant of 200 N/m and a nominal tip radius of 8 nm was used to scan the polished surface of the bone specimens while they were submerged in DI water. The deflection sensitivity of the probe was calibrated on a sapphire sample (SAPPHIRE-12M, Bruker, Billerica, MA). The setpoint was 400 nN; the peak force frequency was 1 kHz; the scan rate was 0.5 Hz. Scans with 3 different sizes of 100, 11, and 6.6 μm were taken. For each size, scans were performed at 3 to 9 different locations. The number of locations being tapped in each scan was 256 × 256.

At each tapping location, cantilever deflection and the vertical position of the AFM tip were recorded. The cantilever deflection can then be related to the load via Hooke's law. This gives

$$F = k\Delta \tag{1}$$

where F is the load; k is the spring constant of the tip cantilever and Δ is the cantilever deflection. The separation, which is the negative of the deformation (i.e. indentation depth), is obtained by adding the vertical position to the cantilever deflection. The load–separation relationship was given by the Derjaguin–Muller–Toporov (DMT) model [21], which has a Hertzian contact profile [22]:

$$F = \frac{4}{3}E^*\sqrt{R^*}\delta^{\frac{3}{2}} \tag{2}$$

where δ is the deformation; E^* is the combined Young's modulus given by $E^* = 1/[(1-{\nu_t}^2)/E_t + (1-{\nu_s}^2)/E_s]$, where E_t and E_s are the elastic moduli of the tip and the substrate, and ν_t and ν_s are the Poisson's ratios of the tip and the substrate, respectively; R^* is the combined radius given by $R^* = R_tR_s/(R_t+R_s)$, where R_t and R_s are the radii of the tip and the substrate, respectively.

In this study, E_t was assumed to be infinite; ν_s was assumed to be 0.3; R_s was assumed to be infinite; The ratio $k/\sqrt{R_t}$ of each AFM probe was calibrated on a highly oriented pyrolytic graphite sample (HOPG-12M, Bruker, Billerica, MA) with a known nominal elastic modulus of 18 GPa. Combining equations (1) and (2), and substituting the above-mentioned variables, the elastic modulus of the substrate at each tapping location was be obtained by fitting the load-deformation curves for the tip retraction processes in NanoScope analysis software (Bruker, Billerica, MA).

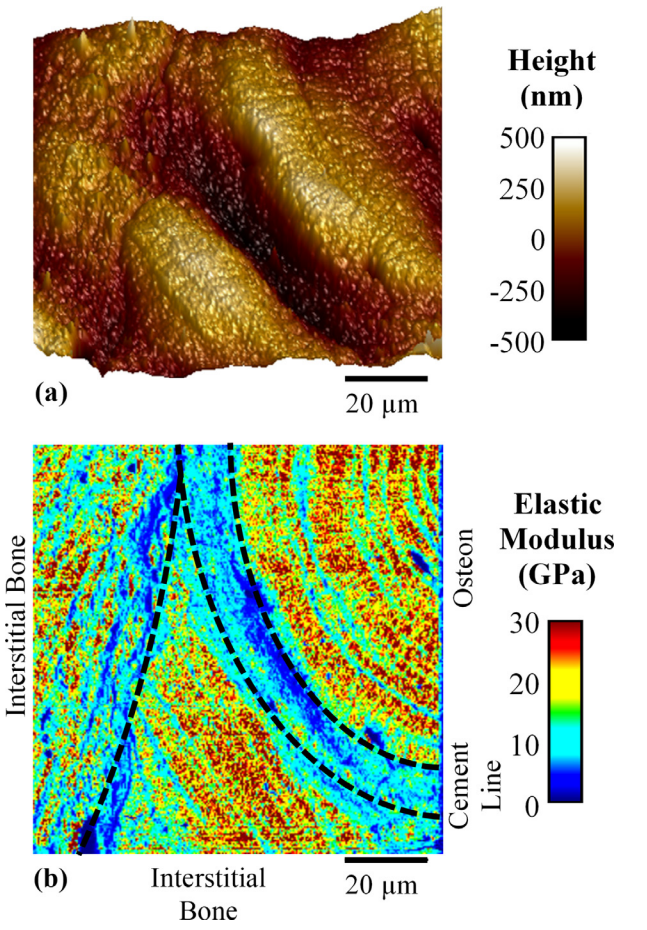

Fig. 1. (a) Surface profile and (b) elastic modulus map of bovine cortical bone showing part of an osteon, interstitial bone and cement line. (Scan size 100 μm).

2.3. Data analysis

4 consecutive 11-μm scans were stitched together manually to present part of an osteon, interstitial bone and the cement lines in between. The elastic modulus values measured from the tapping locations inside these 3 regions were extracted, respectively; average and standard deviation were calculated. Tukey multiple comparison test was performed to compare the mean values among the three groups using Minitab software (Minitab, LLC, State College, PA).

4 other consecutive 11-μm scans were stitched together manually to present the thick and thin lamellae inside an osteon. Tukey comparison test was performed to compare the mean values of elastic moduli of the thick and thin lamellae. Using the OriginLab software (OriginLab Corporation, Northampton, MA), histograms of the elastic moduli inside the thick and thin lamellae regions were calculated and modeled using the summation of multiple general normal distributions, given by

$$n(E_s) = n_0 + \sum_{i=1}^{N} \frac{A_i}{\sigma_i\sqrt{2\pi}} e^{-(E_s-E_i)^2/2\sigma_i^2} \tag{3}$$

where $n(E_s)$ is the number of measurements as a function of elastic modulus; E_i and σ_i is the mean and standard deviation of elastic modulus; A_i is the area under the curve; and n_0 is the offset.

For the 6.6-μm scans, the elastic moduli measured from the mineralized collagen fibril (MCF) bundles and the matrix materials were extracted and compared using Tukey comparison test.

The histograms of the elastic moduli of MCF bundles and the matrix were also modeled the sum of general normal distributions (Eq. (3)), respectively.

3. Results

3.1. Surface profile and elastic modulus map of osteon, interstitial bone and cement line

One of the 100-μm size scans is presented in Fig. 1. It shows part of an osteon, interstitial lamella and cement lines in between. In the elastic modulus map (Fig. 1b), the elastic moduli in osteon and interstitial bone were similar and both ranged from about 16 to 27 GPa. The elastic moduli in the cement lines were much lower than those of osteon and interstitial bone and ranged from about 3 to 11 GPa. The surface morphology in Fig. 1a shows a valley along the cement line between the osteon and the interstitial bone. The interface between the two pieces of interstitial bone was less obvious than the cement line between the osteon and the interstitial bone, in both Fig. 1a and b. The lamellar structures can be observed in the modulus map in Fig. 1b, for both osteon and interstitial bone, but cannot be clearly seen in the surface profile in Fig. 1a.

Four stitched consecutive scans with size of 11 μm × 11 μm are presented in Fig. 2. Generally, the regions with higher elastic modulus are also higher in the surface morphology, and vice versa. But the correspondence did not always exist. For example, the interstitial bone was stiffer than the cement line (Fig. 2b) and was also higher in the surface profile (Fig. 2a). The osteon was also stiffer than the cement line (Fig. 2b), but their heights were not obviously different in the surface profile (Fig. 2a).

The width of the cement lines was ∼5 to 11 μm, as shown in Fig. 2b. The elastic moduli in the osteon, interstitial bone and cement line regions (Fig. 2b) were measured to be 20.51 ± 6.85 GPa (n = 259,920), 21.87 ± 5.48 GPa (n = 131,072), and 7.49 ± 4.23 GPa (n = 32,896), respectively. The differences between each pair were all statistically significant ($P < 0.05$).

3.2. Surface profile and elastic modulus map of thick and thin sub-lamellae

The lamellar structures were observed in both the osteon and the interstitial bone. Four stitched consecutive scans with size of 11 μm × 11 μm are presented in Fig. 3a and b. Both the surface morphology (Fig. 3a) and the elastic modulus map (Fig. 3b) exhibit lamellar structures. However, the patterns in surface morphology (Fig. 3a) and the elastic modulus map (Fig. 3b) do not exactly match. The elastic moduli in the thick and thin sub-lamella in Fig. 3b were measured to be 21.49 ± 6.58 GPa (n = 84,068) and 9.67 ± 2.69 GPa (n = 9104), respectively. Statistically, they are significantly different ($P < 0.05$). The width of the thick sub-lamellae was ∼2.8–13.8 μm; the width of the thin sub-lamellae was ∼1.7–2.4 μm, as measured from elastic modulus map.

Fig. 3c and d present the histograms of elastic moduli measured in the thick and thin sub-lamellae regions, respectively. The histograms were modeled by summations of three general normal distribution functions (Eq. (3)), with the mean values of 10.95 GPa, 15.59 GPa, and 22.86 GPa for thick sub-lamellae and 7.66 GPa, 10.36 GPa, and 13.13 GPa for thin sub-lamellae. The coefficients of determination, R^2, of the curve fittings were both greater than 0.98.

3.3. Surface profile and elastic modulus map of mineralized collagen fibril bundles and matrix

Structures of softer fibril bundles surrounded by harder matrix were observed in both the osteons and the interstitial bone in several 6.6-μm size scans. Representative scans at two different locations are presented in Fig. 4a to d. The mineralized collagen fibril (MCF) bundles show elliptical cross sections with ∼0.58–1.25 μm major axis and ∼0.22–0.49 μm minor axis. In spite of variations in major and minor axes, the aspect ratio is relatively consistent between different bundles, ranging from 2.34 to 2.72. The elastic moduli for the MCF bundles and the matrix, were measured from three 6.6-μm size scans similar to and including Fig. 4b to be 12.94 ± 2.71 GPa (n = 4200) and 28.39 ± 5.75 GPa (n = 7564), respectively. The difference was statistically significant ($p < 0.05$). The MCF bundles were also generally higher than the surrounding matrix in the surface profile (Fig. 4a). However, the patterns in Fig. 4a and b do not exactly match. Moreover, the bundle-matrix patterns have not been observed in the cement line (Fig. 4d) and were not profound in the outermost lamella of an osteon (Fig. 4d), either.

Fig. 4e and f present the histograms of elastic moduli measured in the MCF bundles and the matrix, respectively. The histograms for MCF bundles (Fig. 4e) were modeled by summations of 2 general normal distribution functions (Eq. (3)) with the mean values of 12.48 GPa and 16.90 GPa. The histograms for the matrix (Fig. 4f) were modeled by summations of 4 general normal distribution functions Eq. (3) with the mean values of 20.52 GPa, 25.27 GPa, 29.46 GPa and 34.33 GPa. The coefficients of determination, R^2, of the curve fittings were 0.8 and 0.87, respectively.

4. Discussion

4.1. Hierarchical structures and elastic properties of bone

The results of this study provide elastic properties of bone hierarchical structures at several different scales. Bone in human and other mammals is generally classified into cortical bone and trabecular bone at the macroscopic scale. Cortical bone in the shaft of bovine long bones was characterized in this study. Cortical bone can exhibit osteonal, plexiform, and woven structures at the sub-millimeter scale. In this study, osteons and interstitial bone were observed and characterized. The elastic modulus of the osteons was measured to be 20.51 ± 6.85 GPa and ∼7% lower than that of the interstitial bone (21.87 ± 5.48 GPa). The higher modulus of interstitial bone can be attributed to the fact that interstitial bone was osteons that formed earlier and is more mineralized than the recently-formed osteons. The results are in good agreement with the results in prior works by Rho et al. [10,23]. They tested dry human tibial cortical bone in the longitudinal direction using nanoindentation technique and measured elastic moduli of osteons and interstitial bone to be 22.5 ± 1.3 GPa and 25.8 ± 0.7 GPa, respectively [10,23].

Osteon and interstitial bone both consist of micron-scale lamellar structures. Each lamella is comprised of thick and thin sub-lamellae that have been measured to be ∼5–7 and ∼1 μm in width, respectively [24]. The elastic moduli of thick and thin lamellae in human and bovine long bone have been measured using nanoindentation techniques in prior works [11,25,26]. The elastic modulus of thick lamellae was reported to be between ∼23-27 GPa [11,25,26]. This is in close agreement with the elastic modulus of 21.49 ± 6.58 GPa that was measured in this study. The elastic modulus of thin lamellae was reported to be between ∼20–24 GPa [11,25,26]. This is much higher than the elastic modulus of 9.67 ± 2.69 GPa that was obtained from current work using PeakForce Tapping AFM. The AFM methods

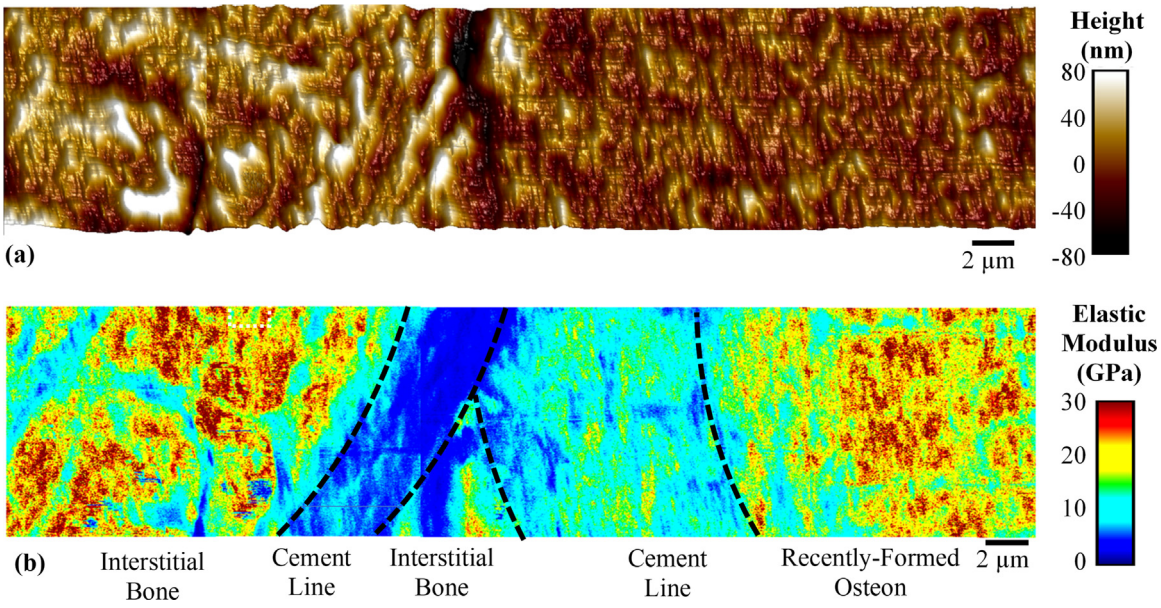

Fig. 2. (a) Surface profile and (b) elastic modulus map of bovine cortical bone. Stitched scans showing osteon, interstitial bone and cement line. (Scan size 11 μm).

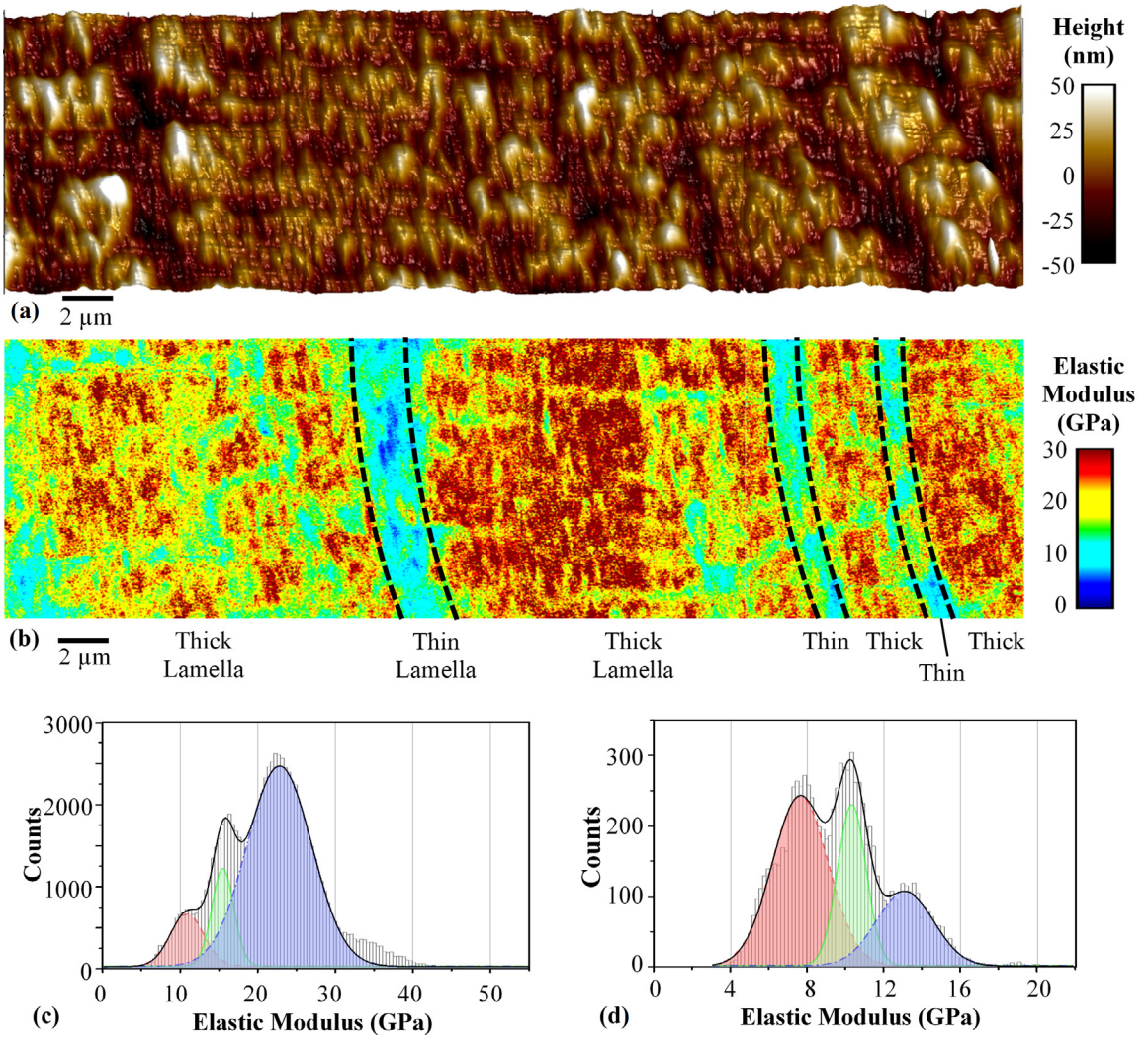

Fig. 3. (a) Surface profile and (b) elastic modulus map of bovine cortical bone. Stitched scans showing thick and thin sub-lamellae in an osteon; Measured and modeled histograms of elastic moduli for (c) thick sub-lamellae and (d) thin sub-lamellae. (Scan size 11 μm).

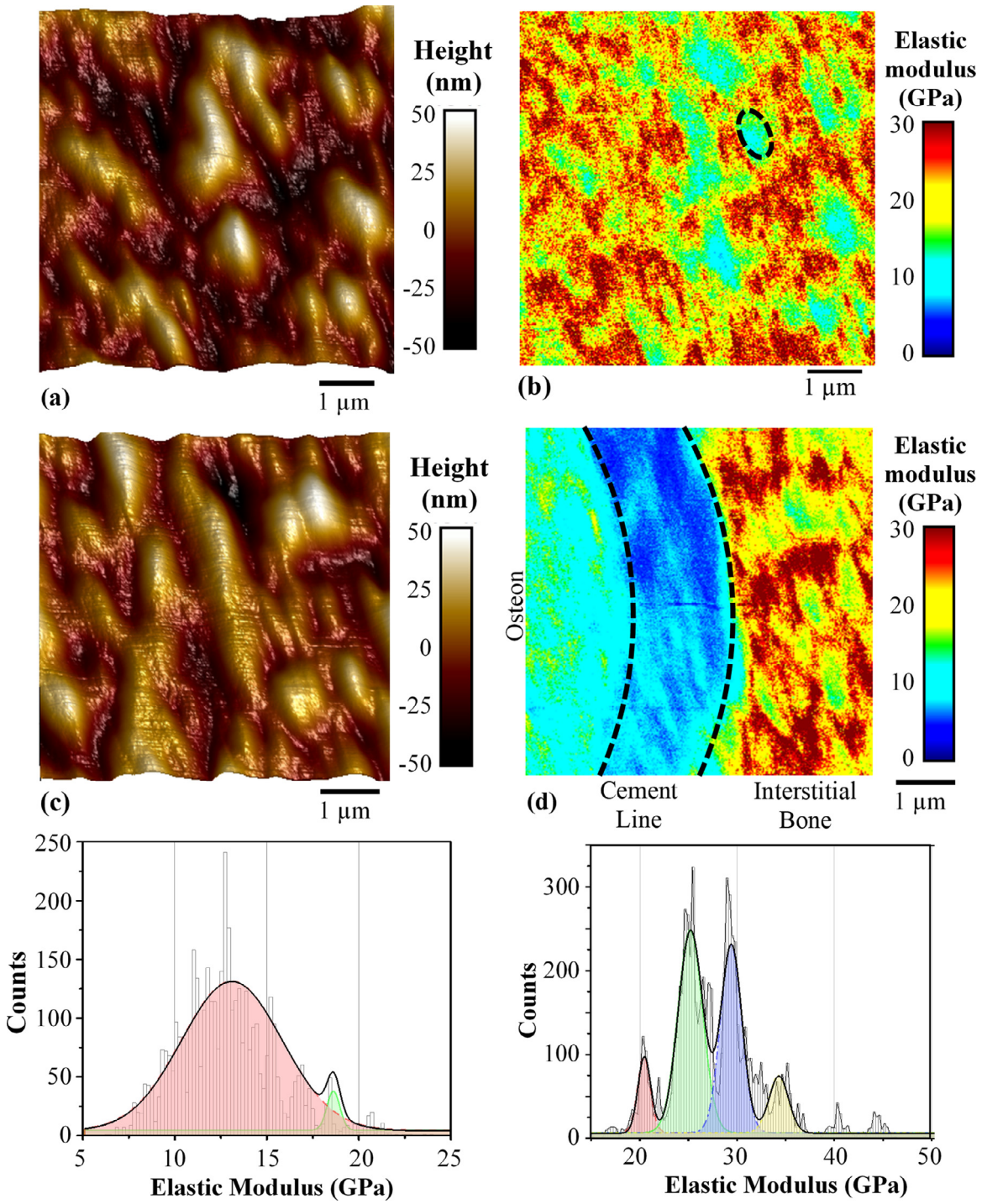

Fig. 4. (a) Surface profile and (b) elastic modulus map of bovine cortical bone showing the mineralized collagen fibril bundles (dashed line) and surrounding matrix; (c) Surface profile and (d) elastic modulus map of bovine cortical bone showing the bundle-matrix patterns in the interstitial bone, which was not shown in the cement line and was not clear at the outermost lamella of an osteon; Measured and modeled histograms of elastic moduli for (e) mineralized collagen fibril bundles and (f) matrix. (Scan size 6.6 μm).

in the current work utilized much lower contact forces that resulted in much smaller contact areas than those in the above-mentioned nanoindentation measurements [11,25,26]. Also, the AFM scans in current work were performed with the specimens submerged in water, unlike the above-mentioned nanoindentation measurements that were performed in air [11,25,26]. The modulus reported in this study is more likely to be the intrinsic elastic modulus of thin lamellae. The variations in the elastic moduli inside single lamella are attributed to the variations in fiber organization [11,26] or degree of mineralization [25].

Another micron-scale structure in cortical bone is cement line. Cement lines are considered to play an important role in the fracture and fatigue behaviors of bone, as they arrest crack growth and absorb energy [27,28]. The strength of cement lines has been measured by single osteon push-out test [5–7]. To the best of our knowledge, current work is the first direct measurement of the elastic modulus of cement lines. The elastic modulus of

cement lines (7.49 ± 4.23 GPa) was measured to be much lower than those for the osteons (20.51 ± 6.85 GPa) and interstitial bone (21.87 ± 5.48 GPa). Some debate still exists regarding the degree of mineralization of cement lines. Burr et al. found that cement lines were less mineralized than the surrounding bone [29]. Skedros et al. reported they were more mineralized than the surrounding bone [30]. More detailed studies of the mineralization and structures of cement lines are required to better understand the mechanical properties of cement lines and their roles in the mechanical behaviors of bone.

Rho et al. reported that the elastic modulus in each lamella reduced from the center towards the outermost of the osteon [31], as measured using nanoindentation. In the elastic map in Fig. 3b, elastic moduli in the outermost thick lamella appeared to be lower than those in the other inner thick lamellae, but more osteons need to be tested in future works, before statistical results can be obtained. It can also be seen that, inside the outermost lamella, the elastic modulus gradually increased from the lower values near the cement lines to higher values towards the Haversian canal (Figs. 2b and 4d). The graduate transition can be attributed to the bone formation and mineralization process at the border of osteons. In contrast, the elastic modulus abruptly increased from the lower values in the cement lines to the higher values in the interstitial bone (Figs. 2b and 4d). The sharp interface can be attributed to the bone resorption process at the border of interstitial bone.

At the submicron-scales, the orientations of mineralized collagen fibril arrays have often been analogized to orthogonal, twisted, rotated, or oscillating plywood structures, depending on the angles of fibril arrays in each lamella [32–37]. Inside some sub-lamellae, there were multiple dominating fibril orientations; Inside the unidirectional sub-lamellae, the preferred fibril orientation maintained nearly constant; In the disordered sub-lamellae, the fibrils did not exhibit preferred orientations [36–38]. The multiple general normal distribution functions in the models for the histograms of elastic moduli in the thick and thin sub-lamellae (Fig. 3c and d) can potentially be attributed to the multiple preferred fibril orientation in each sub-lamella.

There are several theories about the nano-scale ultra-structures of bone. Historically, the mineral crystals have been considered to be located mostly within the fibrils, or mostly between the fibrils, or a combination of both intrafibrillar and interfibrillar [9,39–45]. Recent studies suggested that mineralized collagen fibrils twisted into ∼2-3 μm diameter bundles [46]. The MCF bundles formed into arrays and were surrounded by disordered matrix materials in which the collagen fibrils were randomly oriented [46]. In the ordered MCF bundles, most of mineral located within the fibrils, whereas in the disordered matrix, the mineral was mainly between fibrils [47].

The surface profiles and elastic modulus maps in Fig. 4a–d shows the MCF bundles with ∼1-μm size elliptical cross-sections. In prior works, the elastic modulus of collagen fibrils and MCFs was measured to be 2–7 GPa by tension test of single fibrils [17,18], and was calculated to be 1.3–6.23 GPa by molecular dynamics simulation [48,49]. These are lower than the elastic modulus of 12.94 ± 2.71 GPa measured in the current work. The higher values measured in the current work could be attributed to the wet testing environment and water absorption in the collagen [50]. Moreover, the MCF bundles were measured to be softer than the matrix in the current work. It indicates that the MCF bundles have less mineral content than the matrix, and the intrafibrillar space is smaller than extrafibrillar space.

The histogram for the elastic modulus of MCF bundles (Fig. 4e) was dominated by one general normal distribution, which indicates one dominating angle between the fibrils and the AFM tapping direction, i.e. the long axis of bone. It is consistent with the rope-like twisting fibril structures inside the bundles [47]. In contrast, the 4 general normal distributions in the model for the matrix modulus histogram (Fig. 4f) can be attributed to the random orientations of fibrils, the substantial ground substance, and the sub-micron voids in the disordered matrix materials [46].

4.2. Validity, limitation and future works

In the calculation of elastic modulus in Section 2.2, the deformation of the substrate was assumed to be in the elastic range. Based on the measured elastic moduli results, the contact depth of each tapping was estimated, using Eq. (2), to be less than 5.5 nm. It was also the deformation of the substrate, which was very likely to be in the elastic range. Using Hertzian contact equations [22], the contact patch diameters were also estimated. They were less than 26 nm, which corresponded to the highest (peak) tapping force at the softest tapping location. The spacing between each tapping location was 391, 43, and 26 nm in the scans with sizes of 100, 11, and 6.6 μm, respectively. Hence, the elastic moduli measured in this study can reflect the mechanical properties of the structures as small as dozens of nanometers.

The bovine bone specimens used in this study were kept wet at all time during sample preparation, storage, and testing. The changes in morphology and mechanical property caused by dehydration [51,52] have been minimized. As a comparison, PeakForce Tapping AFM scans were also performed on the same locations shown in Figs. 1–3 in air, after the specimen was blow-dried and then air-dried for ∼12 h. The variations in the elastic modulus in different structures could not be clearly shown in the modulus map.

PeakForce tapping AFM, as a surface characterization method, is sensitive to the surface morphology. The organic-rich regions were likely to be softer than the inorganic-rich regions, hence may be polished off more easily during sample preparation. But, they may absorb more water and swelled up more than the inorganic-rich regions, since the scans were done with specimens submerged in water. Therefore, the surface profiles in Figs. 1–4 cannot directly correlate to the composition variations or the elastic maps. The trends in the surface profiles and elastic maps (Figs. 1–4) do not directly correlate with each other, hence the variations in the resulting elastic maps are attributed to structural and compositional variations. Nevertheless, a direction of future work can be characterizing specimens prepared by other techniques, since the elastic moduli of thick and thin sub-lamellae measured by nanoindentation technique have been shown to be sensitive to different cutting and polishing methods [11].

Another limitation of current work is that tests were only performed on the transverse sectional surface with the tapping direction along the longitudinal bone axis. Considering bone is anisotropic, testing bone surfaces towards other directions is also recommended for future work.

5. Conclusions

This paper presented the results of PeakForce Tapping AFM scans on bovine cortical bone specimens that were submerged in water. The elastic modulus maps of various bone hierarchical structures from submillimeter- to submicron-scales were obtained. The results show that elastic modulus of osteons was slightly lower than the interstitial bone; they were both much stiffer than the cement lines. The elastic modulus in the lamella structures varied periodically from higher values in thick sub-lamellae to the lower values in thin sub-lamellae. The results also show relatively softer MCF bundle arrays embedded in harder matrix materials. The variations in the elastic modulus suggest different degrees of mineralization or different fibril orientations. The histograms of elastic modulus indicate the dominating compositions or dominating fibril orientations.

Declaration of competing interest

The authors declare that they have no known competing financial interests or personal relationships that could have appeared to influence the work reported in this paper.

Acknowledgment

None.

References

[1] A.H. Burstein, J.M. Zika, K.G. Heiple, L. Klein, Contribution of collagen and mineral to the elastic–plastic properties of bone, J. Bone Jt. Surg. Am. 57 (1975) 956–961, http://www.ncbi.nlm.nih.gov/pubmed/1184645.

[2] H.S. Yoon, J. Lawrence Katz, Ultrasonic wave propagation in human cortical bone—II. Measurements of elastic properties and microhardness, J. Biomech. 9 (1976) 459–464, http://dx.doi.org/10.1016/0021-9290(76)90089-0.

[3] W. Bonfield, M.D. Grynpas, Anisotropy of the Young's modulus of bone, Nature 270 (1977) 453–454, http://dx.doi.org/10.1038/270453a0.

[4] K. Choi, J.L. Kuhn, M.J. Ciarelli, S.A. Goldstein, The elastic moduli of human subchondral, trabecular, and cortical bone tissue and the size-dependency of cortical bone modulus, J. Biomech. 23 (1990) 1103–1113, http://dx.doi.org/10.1016/0021-9290(90)90003-L.

[5] A. Ascenzi, E. Bonucci, The shearing properties of single osteons, Anat. Rec. 172 (1972) 499–510, http://dx.doi.org/10.1002/ar.1091720304.

[6] R.F. Bigley, L.V. Griffin, L. Christensen, R. Vandenbosch, Osteon interfacial strength and histomorphometry of equine cortical bone, J. Biomech. 39 (2006) 1629–1640, http://dx.doi.org/10.1016/j.jbiomech.2005.05.006.

[7] X.N. Dong, X. Zhang, X.E. Guo, Interfacial strength of cement lines in human cortical bone, MCB Mech. Chem. Biosyst. (2005) http://dx.doi.org/10.3970/mcb.2005.002.063.

[8] K. Hasegawa, C.H. Turner, D.B. Burr, Contribution of collagen and mineral to the elastic anisotropy of bone, Calcif. Tissue Int. 55 (1994) 381–386, http://dx.doi.org/10.1007/BF00299319.

[9] C.H. Turner, A. Chandran, R.M.V. Pidaparti, The anisotropy of osteonal bone and its ultrastructural implications, Bone 17 (1995) 85–89, http://dx.doi.org/10.1016/8756-3282(95)00148-7.

[10] J.-Y. Rho, T.Y. Tsui, G.M. Pharr, Elastic properties of human cortical and trabecular lamellar bone measured by nanoindentation, Biomaterials 18 (1997) 1325–1330, http://dx.doi.org/10.1016/S0142-9612(97)00073-2.

[11] J. Xu, J.Y. Rho, S.R. Mishra, Z. Fan, Atomic force microscopy and nanoindentation characterization of human lamellar bone prepared by microtome sectioning and mechanical polishing technique, J. Biomed. Mater. Res. 67A (2003) 719–726, http://dx.doi.org/10.1002/jbm.a.10109.

[12] S. Hengsberger, A. Kulik, P. Zysset, A combined atomic force microscopy and nanoindentation technique to investigate the elastic properties of bone structural units, Eur. Cells Mater. 1 (2001) 12–17, http://dx.doi.org/10.22203/eCM.v001a02.

[13] S.J. Eppell, W. Tong, J.L. Katz, L. Kuhn, M.J. Glimcher, Shape and size of isolated bone mineralites measured using atomic force microscopy, J. Orthop. Res. 19 (2001) 1027–1034, http://dx.doi.org/10.1016/S0736-0266(01)00034-1.

[14] T. Hassenkam, G.E. Fantner, J.A. Cutroni, J.C. Weaver, D.E. Morse, P.K. Hansma, High-resolution AFM imaging of intact and fractured trabecular bone, Bone 35 (2004) 4–10, http://dx.doi.org/10.1016/j.bone.2004.02.024.

[15] J.H. Kindt, P.J. Thurner, M.E. Lauer, B.L. Bosma, G. Schitter, G.E. Fantner, M. Izumi, J.C. Weaver, D.E. Morse, P.K. Hansma, In situ observation of fluoride-ion-induced hydroxyapatite–collagen detachment on bone fracture surfaces by atomic force microscopy, Nanotechnology 18 (2007) 135102, http://dx.doi.org/10.1088/0957-4484/18/13/135102.

[16] K. Tai, H.J. Qi, C. Ortiz, Effect of mineral content on the nanoindentation properties and nanoscale deformation mechanisms of bovine tibial cortical bone, J. Mater. Sci. Mater. Med. 16 (2005) 947–959, http://dx.doi.org/10.1007/s10856-005-4429-9.

[17] J.A.J. van der Rijt, K.O. van der Werf, M.L. Bennink, P.J. Dijkstra, J. Feijen, Micromechanical testing of individual collagen fibrils, Macromol. Biosci. 6 (2006) 697–702, http://dx.doi.org/10.1002/mabi.200600063.

[18] F. Hang, A.H. Barber, Nano-mechanical properties of individual mineralized collagen fibrils from bone tissue, J. R. Soc. Interface 8 (2011) 500–505, http://dx.doi.org/10.1098/rsif.2010.0413.

[19] M. Stolz, R. Raiteri, A.U. Daniels, M.R. VanLandingham, W. Baschong, U. Aebi, Dynamic elastic modulus of porcine articular cartilage determined at two different levels of tissue organization by indentation-type atomic force microscopy, Biophys. J. 86 (2004) 3269–3283, http://dx.doi.org/10.1016/S0006-3495(04)74375-1.

[20] K. Tai, M. Dao, S. Suresh, A. Palazoglu, C. Ortiz, Nanoscale heterogeneity promotes energy dissipation in bone, Nature Mater. 6 (2007) 454–462, http://dx.doi.org/10.1038/nmat1911.

[21] B.V. Derjaguin, V.M. Muller, Y.P. Toporov, Effect of contact deformations on the adhesion of particles, J. Colloid Interface Sci. 53 (1975) 314–326, http://dx.doi.org/10.1016/0021-9797(75)90018-1.

[22] V.H.H. Hertz, Ueber die Berührung fester elastischer Körper, J. Reine Angew. Math. (Crelle's J.) (1882) 156–171, http://dx.doi.org/10.1515/crll.1882.92.156.

[23] J.-Y. Rho, M.E. Roy, T.Y. Tsui, G.M. Pharr, Elastic properties of microstructural components of human bone tissue as measured by nanoindentation, J. Biomed. Mater. Res. 45 (1999) 48–54, http://dx.doi.org/10.1002/(SICI)1097-4636(199904)45:1<48::AID-JBM7>3.0.CO;2-5.

[24] A. Ardizzoni, Osteocyte lacunar size–lamellar thickness relationships in human secondary osteons, Bone 28 (2001) 215–219, http://dx.doi.org/10.1016/S8756-3282(00)00417-8.

[25] H.S. Gupta, U. Stachewicz, W. Wagermaier, P. Roschger, H.D. Wagner, P. Fratzl, Mechanical modulation at the lamellar level in osteonal bone, J. Mater. Res. 21 (2006) 1913–1921, http://dx.doi.org/10.1557/jmr.2006.0234.

[26] D. Carnelli, P. Vena, M. Dao, C. Ortiz, R. Contro, Orientation and size-dependent mechanical modulation within individual secondary osteons in cortical bone tissue, J. R. Soc. Interface 10 (2013) 20120953, http://dx.doi.org/10.1098/rsif.2012.0953.

[27] F.J. O'Brien, D. Taylor, T.C. Lee, Microcrack accumulation at different intervals during fatigue testing of compact bone, J. Biomech. (2003) http://dx.doi.org/10.1016/S0021-9290(03)00066-6.

[28] K.J. Koester, J.W. Ager, R.O. Ritchie, The true toughness of human cortical bone measured with realistically short cracks, Nature Mater. 7 (2008) 672–677, http://dx.doi.org/10.1038/nmat2221.

[29] D.B. Burr, M.B. Schaffler, R.G. Frederickson, Composition of the cement line and its possible mechanical role as a local interface in human compact bone, J. Biomech. 21 (1988) 939–945, http://dx.doi.org/10.1016/0021-9290(88)90132-7.

[30] J.G. Skedros, J.L. Holmes, E.G. Vajda, R.D. Bloebaum, Cement lines of secondary osteons in human bone are not mineral-deficient: New data in a historical perspective, Anat. Rec. - A Discov. Mol. Cell. Evol. Biol. (2005) http://dx.doi.org/10.1002/ar.a.20214.

[31] J.Y. Rho, P. Zioupos, J.D. Currey, G.M. Pharr, Variations in the individual thick lamellar properties within osteons by nanoindentation, Bone 25 (1999) 295–300, http://dx.doi.org/10.1016/S8756-3282(99)00163-5.

[32] A. Ascenzi, E. Bonucci, The compressive properties of single osteons, Anat. Rec. 161 (1968) 377–391, http://dx.doi.org/10.1002/ar.1091610309.

[33] Y. Bouligand, Twisted fibrous arrangements in biological materials and cholesteric mesophases, Tissue Cell 4 (1972) 189–217, http://dx.doi.org/10.1016/S0040-8166(72)80042-9.

[34] M.M. Giraud-Guille, Twisted plywood architecture of collagen fibrils in human compact bone osteons, Calcif. Tissue Int. 42 (1988) 167–180, http://dx.doi.org/10.1007/BF02556330.

[35] S. Weiner, T. Arad, W. Traub, Crystal organization in rat bone lamellae, FEBS Lett. 285 (1991) 49–54, http://dx.doi.org/10.1016/0014-5793(91)80722-F.

[36] S. Weiner, T. Arad, I. Sabanay, W. Traub, Rotated plywood structure of primary lamellar bone in the rat: Orientations of the collagen fibril arrays, Bone 20 (1997) 509–514, http://dx.doi.org/10.1016/S8756-3282(97)00053-7.

[37] P. Varga, A. Pacureanu, M. Langer, H. Suhonen, B. Hesse, Q. Grimal, P. Cloetens, K. Raum, F. Peyrin, Investigation of the three-dimensional orientation of mineralized collagen fibrils in human lamellar bone using synchrotron X-ray phase nano-tomography, Acta Biomater. 9 (2013) 8118–8127, http://dx.doi.org/10.1016/j.actbio.2013.05.015.

[38] N. Reznikov, R. Almany-Magal, R. Shahar, S. Weiner, Three-dimensional imaging of collagen fibril organization in rat circumferential lamellar bone using a dual beam electron microscope reveals ordered and disordered sub-lamellar structures, Bone 52 (2013) 676–683, http://dx.doi.org/10.1016/j.bone.2012.10.034.

[39] J.D. Currey, The relationship between the stiffness and the mineral content of bone, J. Biomech. 2 (1969) 477–480, http://dx.doi.org/10.1016/0021-9290(69)90023-2.

[40] E.P. Katz, S.-T. Li, Structure and function of bone collagen fibrils, J. Mol. Biol. 80 (1973) 1–15, http://dx.doi.org/10.1016/0022-2836(73)90230-1.

[41] L.C. Bonar, S. Lees, H.A. Mook, Neutron diffraction studies of collagen in fully mineralized bone, J. Mol. Biol. 181 (1985) 265–270, http://dx.doi.org/10.1016/0022-2836(85)90090-7.

[42] N. Sasaki, A. Tagami, T. Goto, M. Taniguchi, M. Nakata, K. Hikichi, Atomic force microscopic studies on the structure of bovine femoral cortical bone at the collagen fibril-mineral level, J. Mater. Sci. Mater. Med. 13 (2002) 333–337, http://dx.doi.org/10.1023/A:1014079421895.

[43] E.A. McNally, H.P. Schwarcz, G.A. Botton, A.L. Arsenault, A model for the ultrastructure of Bone based on electron microscopy of Ion-Milled sections, PLoS One 7 (2012) e29258, http://dx.doi.org/10.1371/journal.pone.0029258.

[44] B. Alexander, T.L. Daulton, G.M. Genin, J. Lipner, J.D. Pasteris, B. Wopenka, S. Thomopoulos, The nanometre-scale physiology of bone: steric modelling and scanning transmission electron microscopy of collagen–mineral structure, J. R. Soc. Interface 9 (2012) 1774–1786, http://dx.doi.org/10.1098/rsif.2011.0880.

[45] E. McNally, F. Nan, G.A. Botton, H.P. Schwarcz, Scanning transmission electron microscopic tomography of cortical bone using Z-contrast imaging, Micron. 49 (2013) 46–53, http://dx.doi.org/10.1016/j.micron.2013.03.002.

[46] N. Reznikov, R. Shahar, S. Weiner, Three-dimensional structure of human lamellar bone: The presence of two different materials and new insights into the hierarchical organization, Bone 59 (2014) 93–104, http://dx.doi.org/10.1016/j.bone.2013.10.023.

[47] N. Reznikov, R. Shahar, S. Weiner, Bone hierarchical structure in three dimensions, Acta Biomater. 10 (2014) 3815–3826, http://dx.doi.org/10.1016/j.actbio.2014.05.024.

[48] M.J. Buehler, Molecular nanomechanics of nascent bone: fibrillar toughening by mineralization, Nanotechnology 18 (2007) 295102, http://dx.doi.org/10.1088/0957-4484/18/29/295102.

[49] A.K. Nair, A. Gautieri, S.-W. Chang, M.J. Buehler, Molecular mechanics of mineralized collagen fibrils in bone, Nature Commun. 4 (2013) 1724, http://dx.doi.org/10.1038/ncomms2720.

[50] R. Harley, D. James, A. Miller, J.W. White, Phonons and the elastic moduli of collagen and muscle [38], Nature (1977) http://dx.doi.org/10.1038/267285a0.

[51] J.Y. Rho, G.M. Pharr, Effects of drying on the mechanical properties of bovine femur measured by nanoindentation., J. Mater. Sci. Mater. Med. 10 (1999) 485–488, http://dx.doi.org/10.1023/A:1008901109705.

[52] L. Feng, M. Chittenden, J. Schirer, M. Dickinson, I. Jasiuk, Mechanical properties of porcine femoral cortical bone measured by nanoindentation, J. Biomech. 45 (2012) 1775–1782, http://dx.doi.org/10.1016/j.jbiomech.2012.05.001.